SAND2017-11537C

# Using High-Resolution Measurements to Update Finite Element Substructure Models

Daniel P. Rohe
Structural Dynamics Department
Sandia National Laboratories*
P.O. Box 5800 - MS0557
Albuquerque, NM, 87185
dprohe@sandia.gov

**ABSTRACT**

Many methods have been proposed for updating finite element matrices using experimentally derived modal parameters. By using these methods, a finite element model can be made to exactly match the experiment. These techniques have not achieved widespread use in finite element modeling because they introduce non-physical matrices. Recently, Scanning Laser Doppler Vibrometery (SLDV) has enabled finer measurement point resolution and more accurate measurement point placement with no mass loading compared to traditional accelerometer or roving hammer tests. Therefore, it is worth reinvestigating these updating procedures with high-resolution data inputs to determine if they are able to produce finite element models that are suitable for substructuring. A rough finite element model of an Ampair Wind Turbine Blade was created, and a SLDV measurement was performed that measured three-dimensional data at every node on one surface of the blade. This data was used to update the finite element model so that it exactly matched test data. A simple substructuring example of fixing the base of the blade was performed and compared to previously measured fixed-base data.

Keywords: 3D, SLDV, Model Updating, Modal

## 1 INTRODUCTION

The model updating problem has been well-visited through the history of experimental structural dynamics. Many techniques have been proposed in which finite element matrices can be directly updated to exactly match test data, for example [1-3]. Such "direct" updating techniques have not achieved widespread acceptance at Sandia National Laboratories. Issues with these techniques include non-physical mass and stiffness matrices which leads to modes not in the updated set becoming spurious. This can result in erroneous results, especially in substructuring applications where a change in boundary conditions of the test article often requires a number of higher frequency modes for a good approximation of a fixed-base shape.

Scanning Laser Doppler Vibrometry (SLDV) has been shown to have advantages over traditional mounted sensors [4]. For example, it allows for non-contact measurements which do not mass-load the test article. Additionally, a finer measurement point resolution can often be achieved through the use of scanning mirrors in the laser heads which are much more precise than a roving hammer or roving accelerometer test. SLDV therefore has the potential to supply a finite element model (FEM) a larger volume of data at more precisely located measurement points. 3D SLDV can also provide three-dimensional data at each measurement point. This work investigates the use of 3D SLDV to provide data to update a rough finite element model for use in substructuring applications through a case study on a Ampair 600 Wind Turbine Blade [5,6].

## 2 PRELIMINARY FINITE ELEMENT MODEL

* Sandia National Laboratories is a multimission laboratory managed and operated by National Technology and Engineering Solutions of Sandia LLC, a wholly owned subsidiary of Honeywell International Inc. for the U.S. Department of Energy's National Nuclear Security Administration under contract DE-NA0003525.

A rough finite element model was created from the solid geometry provided by Nurbhai and Macknelly [7]. To facilitate efficient investigation into model updating approaches, the FEM was created such that it would run on a typical desktop computer in a reasonable amount of time. While a FEM of the entire blade and hub assembly was created, only a single blade was investigated here. The single blade FEM consisted of two element blocks, the solid "core" of the blade, consisting of 4681 tetrahedral elements and a thin "skin" consisting of 2570 triangular shell elements. The model contained 1504 nodes, of which the skin nodes had six degrees of freedom each whereas the nodes found only in the core contained only three degrees of freedom. Figure 1 shows the finite element model. With only one or two elements through the thickness of the blade core, the model was almost certainly not converged. The initial material properties were not known a priori, so these were updated after the experimental data was taken.

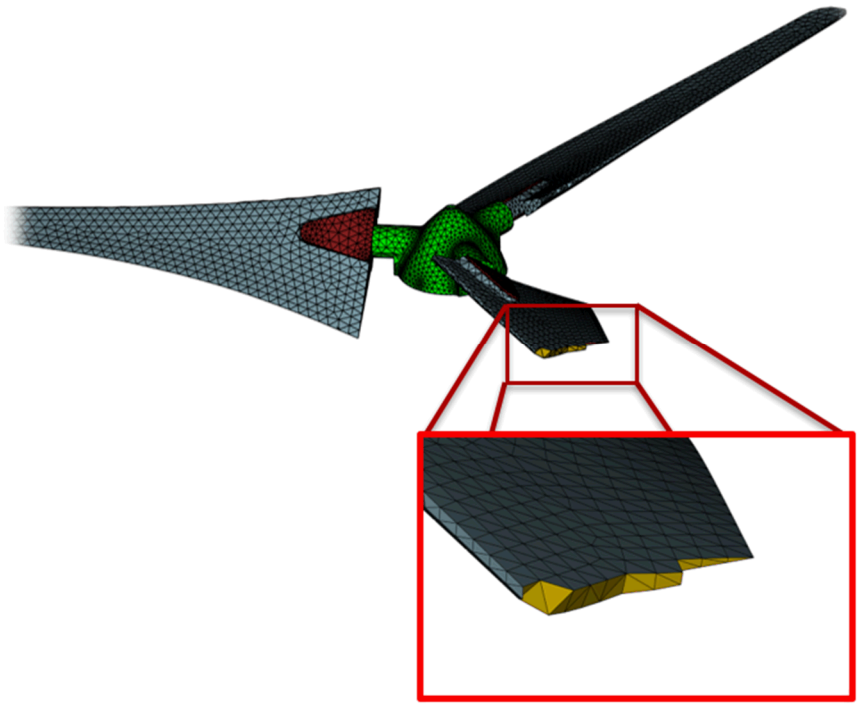

**Figure 1: Rough finite element model for use in this investigation with one blade shown cut away to reveal element sparsity through the thickness.**

## 3 EXPERIMENTAL MODAL TEST AND ANALYSIS

Rather than needing to deal with some interpolation scheme between the experimental data and the FEM, it was decided to place the measurement points on the blade at the locations of the nodes in the FEM. The nodes to scan were chosen from the set of nodes on one side of the finite element model at least 1.27 cm (0.5 in) from the edge of the blade with an angle of incidence of less than 60 degrees to the axis of rotation of the hub.

**Figure 2: Blade Scan Points shown on the Finite Element Model**

### 3.1 Laser Alignment

Before the measurement points could be placed on the blade, the laser system had to be aligned with the part. Unfortunately, due to their popularity as a test bed structure, the blades had seen a lot of use and abuse in the structural dynamics laboratory.

All of the sharp corners on the blade that would have been useful for alignment were damaged, so some other datum would be necessary to align the blade.

Alignment points were drawn over each blade as well as the hub. The entire blade-hub assembly was used for this portion of the alignment because it was thought that if the alignment was performed over a larger area, the alignment error could be minimized. Approximately 40 points were spread over each blade (Figure 5), but at this point the locations of these points in the blade coordinate system were not known, and due to the blade geometry they could not be easily measured using standard tools such as a ruler or compass and protractor. Instead, the 3D SLDV was used in a slightly nonstandard way to determine the locations of the points. The 3D SLDV system was aligned to an arbitrary coordinate system using the provided reference object. The blade-hub assembly was then placed in the coordinate system and the alignment points were triangulated using the laser vibrometer system. The $(x, y, z)$ coordinates of the alignment points in this arbitrary coordinate system could then be extracted from the laser system. However, these coordinates were not yet aligned with the FEM coordinate system.

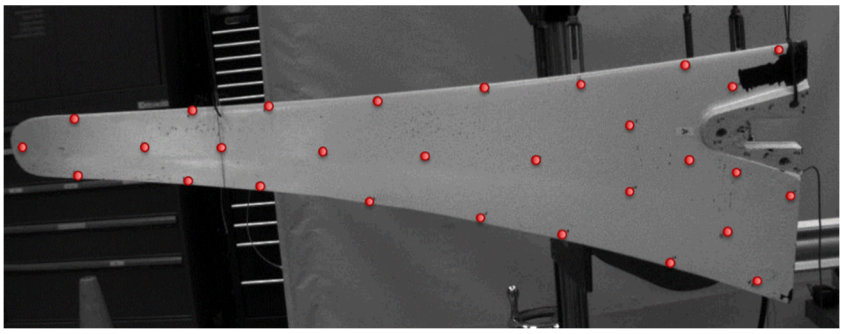

**Figure 3: Alignment point locations on the blade**

To align the arbitrary alignment point coordinate system with the FEM coordinate system, the alignment points were exported into MATLAB for analysis. The goal of this analysis was to determine a transformation matrix **T** that would transform the alignment point coordinates into the finite element model coordinates. More precisely, the goal was to determine the transformation **T** that would result in the minimum sum-squared distance of the alignment points to the surface of the FEM (see Figure 4). The alignment points were initially rotated and translated compared to the finite element model (Figure 5), so any type of algorithmic optimization of the transformation matrix at this point would likely result in an incorrect local optimum rather than the global optimum. To give the search algorithm a better chance at locating the true minimum, the alignment points were transformed using a trial-and-error process to get the alignment points close to the surface (Figure 6).

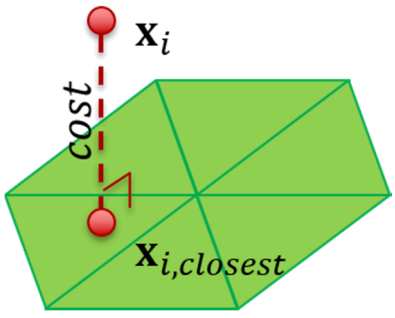


$$cost = \sum_{i=1}^{n_{points}} \left\| \mathbf{x}_i - \mathbf{x}_{i,closest} \right\|^2$$

**Figure 4: Schematic showing the cost function to be minimized, where the cost relates to the distance of the point $x_i$ to the closest point on the FEM surface $x_{i,closest}$.**

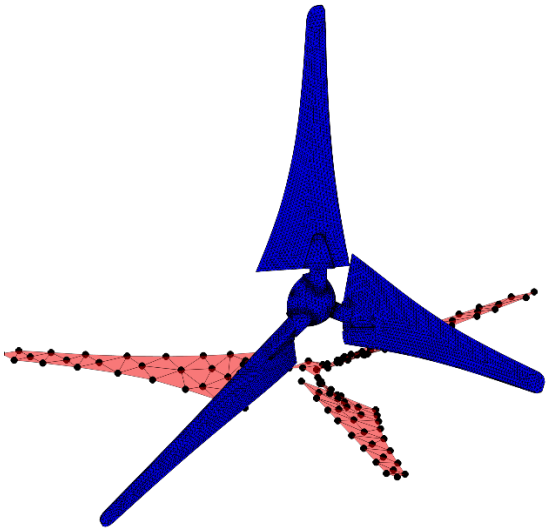

**Figure 5: Initial alignment point locations compared to FEM model**

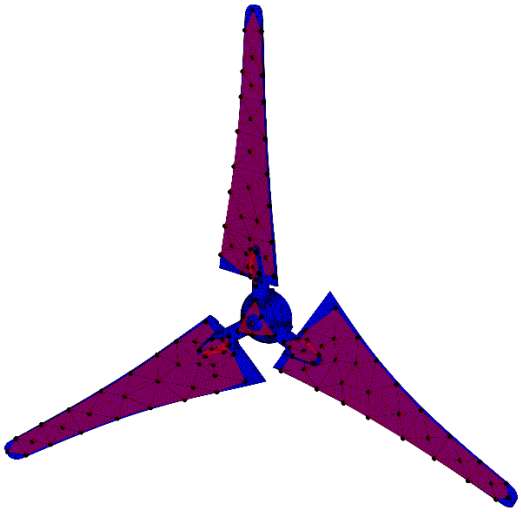

**Figure 6: Closer alignment point locations compared to FEM model**

With the initial conditions close to the optimal conditions, the FEM and Alignment point geometry could be passed into a cost function that could be optimized, with the additional parameters of three rotations and three translations to be optimized. This cost function computes the distance from each alignment point to the closest point on the structure. The problem of finding the closest point on a triangle to a different point in space is a straightforward geometric problem; however searching all triangles to determine which is the closest point is inefficient. To increase efficiency, the finite element model was culled to consist of only those elements that were close to an alignment point (Figure 7). The cost function was then passed to the nonlinear optimization function `fminsearch` in MATLAB which determined the rotations and translations that resulted in the minimum distance of the alignment points from the FEM surface. This transformation was then applied to the alignment point coordinates, which resulted in the alignment point coordinates in the FEM coordinate system. With the updated coordinates, these alignment points could be used as the alignment data for the 3D SLDV system. With the laser system aligned to the FEM coordinate system, the FEM nodal coordinates shown in Figure 2 could be directly imported into the laser software to serve as the measurement points, shown in Figure 8.

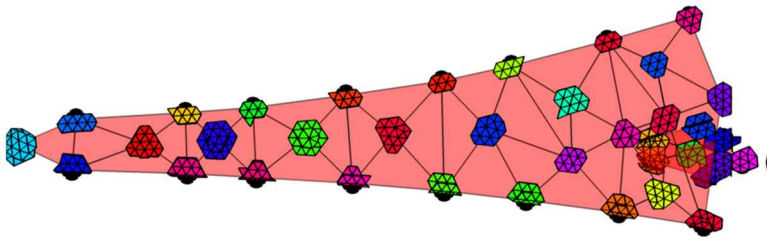

**Figure 7: Reduced set of triangles for computing the closest distance.**

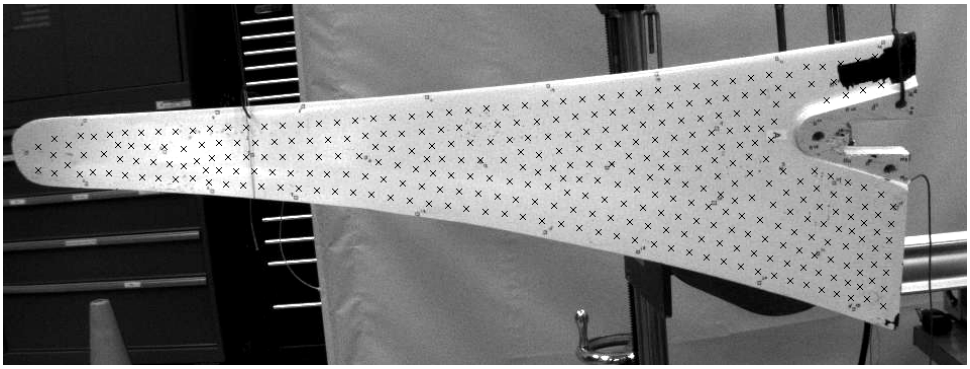

**Figure 8: Measurement points on the blade marked with × symbols.**

### 3.2 Blade Testing and Preliminary FEM Updating

A shaker and drive point accelerometer were attached to a single Ampair blade on the opposite side of the scan points, and pseudorandom excitation was applied to the part. 359 points were measured on the blade. 10 elastic modes were extracted from the blade below 800 Hz using the Synthesize Modes and Correlate (SMAC) algorithm [8]. A Complex Mode Indictor Function (CMIF) showing the experimental data and analytical fits is shown in Figure 9.

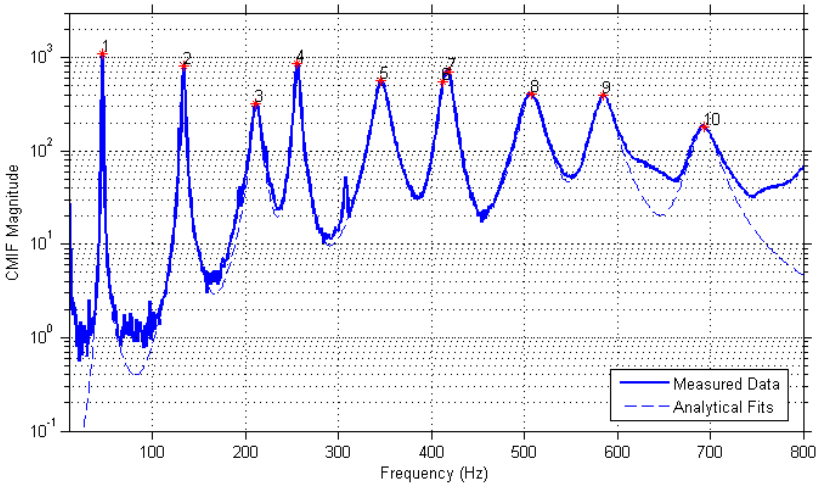


**Figure 9: Analytical Modal Fits compared to Experimental Data**

This preliminary modal data was used to tune the material parameters of the rough FEM discussed in Section 2. A Poisson's ratio of 0.3 was assumed. The density of the core and skin material was assigned using the system of equations relating total mass and lengthwise center of gravity. The Young's modulus of each material was assigned via another nonlinear optimization using the `fminsearch` function. Here the cost function was set up so that with each iteration of the optimization, the Young's modulus of each material was passed as a parameter to the function and an eigenvalue finite element analysis was performed that solved for the first 10 elastic natural frequencies of the blade. The cost was defined as the sum squared percent error in natural frequencies. Note that no shape-based correlation of natural frequencies was used to pair corresponding shapes; if modes were out of order, then the natural frequencies would be miscorrelated. This can be seen in the flipping of the 3rd bending and torsion modes of the FEM and experimental data. Experimental and Preliminary FEM modal parameters are summarized in Table 1. The modal assurance criterion (MAC) matrix is shown in Figure 10. The first two elastic shapes show good correlation between test and FEM, but higher modes show a lower degree of correlation.

**Table 1: Summary of Experimental and Finite Element Modal Parameters**

| Exp Mode | Exp Frequency | Prelim FEM Mode | Prelim FEM Freq |
|---|---|---|---|
| 1st Bending | 46.0 Hz | 1st Bending | 46.0 Hz |

| | | | |
|---|---|---|---|
| 2nd Bending | 133 Hz | 2nd Bending | 127 Hz |
| 1st Torsion | 211 Hz | 3rd Bending | 240 Hz |
| 3rd Bending | 255 Hz | 1st Torsion | 247 Hz |
| 2nd Torsion | 346 Hz | 1st Edgwise | 346 Hz |
| 4th Bending | 418 Hz | 4th Bending | 381 Hz |

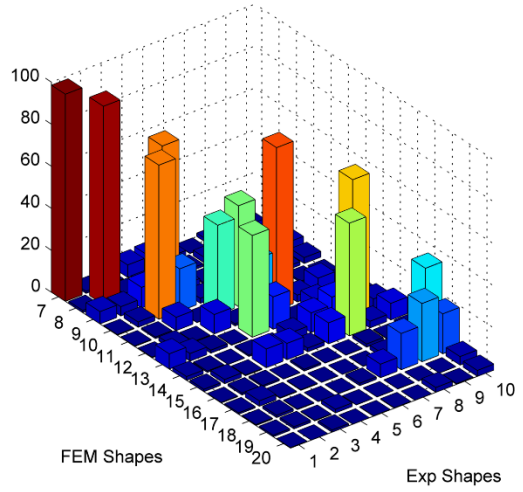


**Figure 10: Modal Assurance Criterion Matrix**

## 4 FINITE ELEMENT MODEL UPDATING

Three model updating techniques were investigated for this case study. The first was the Berman and Nagy approach [2] and the second was the Analytical Model Improvement (AMI) method of O'Callahan [3]. The final approach utilized the Variability Improvement of Key Inaccurate Node Groups (VIKING) [9] technique and was the same process used in [10]. The end goal is to be able to use the updated finite element model in substructuring applications. For this case study, that will consist of fixing the base of the blade to approximate the fixed-base modes of the structure.

The model updating is performed using MATLAB to modify the finite element matrices, which were exported from the finite element code. It is important to fully understand which degrees of freedom correspond to which rows and columns of the matrices, as well as to understand how the matrices are populated. For example, in the Sierra/Structural Dynamics code that was used for this effort, the degrees of freedom were sorted numerically by node number. A confounding aspect, however, was that the nodes have a variable number of degrees of freedom. In order to map the experimental degrees of freedom to the FEM degrees of freedom, the nodes first had to be binned by whether they were contained in shell elements (triangular elements on the skin) or not. These shell elements would have rotational degrees of freedom and therefore have six rows and columns in the matrix per node rather than only three. A good practice that was employed during this effort was to compute the eigenvectors (mode shapes) of the mass and stiffness matrices in MATLAB for one or two modes (even with large matrices this is not terribly computationally intensive because the eigenvalues were already known from the FEM eigensolution). Then, if the eigenvectors appeared correct when plotted, one could have a good deal of confidence that the book-keeping of the FEM matrices was performed correctly.

### 4.1 Berman-Nagy Approach

As a first attempt at updating a finite element model to match test data, the Berman Nagy Approach was used. This approach directly modifies the mass and stiffness matrices of the finite element model per the following equations:

$$\boldsymbol{M} = \boldsymbol{M}_A + \boldsymbol{M}_A\, \boldsymbol{\Phi}\, m_A^{-1}(\boldsymbol{I} - m_A)m_A^{-1}\, \boldsymbol{\Phi}^T\, \boldsymbol{M}_A \tag{1}$$

$$\mathbf{K} = \mathbf{K}_{\boldsymbol{A}} + (\boldsymbol{\Delta} + \boldsymbol{\Delta}^{\boldsymbol{T}}) \tag{2}$$

$$\boldsymbol{\Delta} = \frac{\mathbf{1}}{\mathbf{2}}\mathbf{M}\boldsymbol{\Phi}(\boldsymbol{\Phi}^{\boldsymbol{T}}\mathbf{K}_{\boldsymbol{A}}\boldsymbol{\Phi} + \boldsymbol{\Omega}^{\mathbf{2}})\boldsymbol{\Phi}^{\boldsymbol{T}}\mathbf{M} - \mathbf{K}_{\boldsymbol{A}}\boldsymbol{\Phi}\boldsymbol{\Phi}^{\boldsymbol{T}}\mathbf{M} \tag{3}$$

where $\boldsymbol{\Phi}$ is the experimental mode shape matrix, expanded to the full finite element degrees of freedom, $\mathbf{M}_A$ is the FEM mass matrix, $\mathbf{K}_A$ is the FEM stiffness matrix, $\boldsymbol{\Omega}^2 = [\ddots\ \omega^2\ \ddots]$ is the diagonal experimental eigenvalue matrix, $m_A = \boldsymbol{\Phi}^T\mathbf{M}_A\boldsymbol{\Phi}$ is the normalized generalized mass matrix, and $\mathbf{I}$ is the identity matrix.

In order to apply equations (1) and (3), the experimental mode shape matrix must first be expanded to the full finite element degrees of freedom. This was done using Guyan expansion:

$$\mathbf{K}_A = \begin{bmatrix} \mathbf{K}_{aa} & \mathbf{K}_{ad} \\ \mathbf{K}_{da} & \mathbf{K}_{dd} \end{bmatrix} \tag{4}$$

$$\mathbf{T}_s = \begin{bmatrix} \mathbf{I} \\ -\mathbf{K}_{dd}^{-1}\mathbf{K}_{da} \end{bmatrix} \tag{5}$$

$$\boldsymbol{\Phi} = \mathbf{T}_s\boldsymbol{\Phi}_a \tag{6}$$

where $a$ represents the degrees of freedom present in the measurement, $d$ represents the degrees of freedom not present in the measurement, and $\boldsymbol{\Phi}_a$ are the mode shapes from the experiment.

As is the case with any experimental data, and perhaps especially with laser vibrometer data where optical issues such as signal dropout or speckle noise can occur, measurement error can contaminate the results. To smooth out some of the noise, the experimental shapes were projected to the space spanned by the first 100 finite element shapes as shown in (7).

$$\widetilde{\boldsymbol{\Phi}}_a = \boldsymbol{\Phi}_{a,fem}\boldsymbol{\Phi}_{a,fem}^{+}\boldsymbol{\Phi}_a \tag{7}$$

The smoothed finite element shapes $\widetilde{\boldsymbol{\Phi}}_a$ were then used in (6) to expand to the full set of degrees of freedom. The mass and stiffness matrices were then updated per (1) and (3). To verify that the updating process was performed correctly, the eigenvalue problem was solved for the elastic modes of the system corresponding to the experimental modes. The eigenvalue problem is more computationally intensive now that the $\mathbf{M}$ and $\mathbf{K}$ matrices are full from the updating process. It was found that though the FEM system contained eigenvalues and eigenvectors that exactly matched the experimental values, other eigenvalues of the system were now unphysical. For example, the rigid body modes, which are nominally at 0 Hz, now had non-zero stiffness. Other spurious modes also appeared in the bandwidth of interest. Figure 11 shows a representative frequency response function of the free-free FEM.

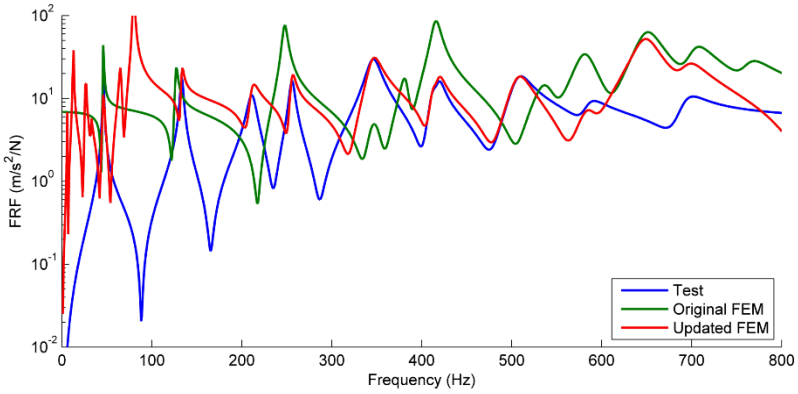


**Figure 11: Representative frequency response function for the updated FEM via the Berman-Nagy approach. Note the rigid body natural frequencies up to nearly 100 Hz and the spurious mode near 650 Hz.**

Clearly, as the rigid body modes play a large role in the substructuring calculations especially for low frequency modes [11], matching fixed base results with such a model seemed unlikely. The updating procedure was performed a second time, where the expanded experimental modes $\widetilde{\boldsymbol{\Phi}}_a$ were supplemented with the FEM rigid body modes. In this case, the rigid body mode shapes and natural frequencies would be forced to be reasonable by the updating procedure. A representative frequency response function is shown in Figure 12.

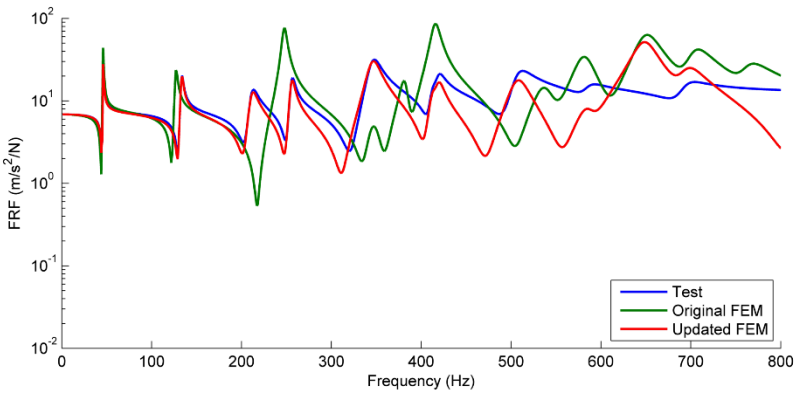


**Figure 12: Representative frequency response function for the updated FEM via the Berman-Nagy approach with FEM rigid body modes included as target modes.**

With the updated mass and stiffness matrices, the base of the blade was constrained to make a fixed base structure. The natural frequencies were compared to those in [6] using a fixed base configuration. To judge the effectiveness of the technique in improving the fixed base prediction, the results were compared against the fixed base prediction using only the non-updated finite element model. These results are shown in Table 2.

**Table 2: Fixed base FEM predictions using the Berman-Nagy updating approach. The truth column contains the average of the natural frequencies found in [6].**

| Mode | Truth | Non-updated FEM | Updated FEM only Experiment | Updated FEM Exp + RBM |
|---|---|---|---|---|
| 1 | 20.1 Hz | 19.3 Hz | 41.5 Hz | 31.5 Hz |
| 2 | 70.2 Hz | 70.7 Hz | 76.7 Hz | 74.5 Hz |
| 3 | 131 Hz | 141 Hz | 165 Hz | 161 Hz |

The coarse and poorly-correlated FEM still did reasonably well at predicting the fixed base natural frequencies. When the Berman-Nagy approach was used without including the analytical FEM rigid body modes, the predicted fixed base natural frequencies were terrible with over 100% error on the first natural frequency. The predictions improved drastically when the rigid body modes were included in the updating procedure; however, the results were still not as good as the non-updated FEM.

### 4.2 Analytical Model Improvement Approach

The same updating procedure was attempted using the AMI approach. This approach directly modifies the mass and stiffness matrices of the finite element model using the following equations:

$$\mathbf{M} = \mathbf{M}_A + \mathbf{V}^T(\mathbf{I} - \bar{\mathbf{M}}_A)\mathbf{V} \tag{8}$$

$$\mathbf{K} = \mathbf{K}_A + \mathbf{V}(\boldsymbol{\Omega}^2 + \bar{\mathbf{K}}_A)\mathbf{V} - \left((\mathbf{K}_A\boldsymbol{\Phi}\mathbf{V}) - (\mathbf{K}_A\boldsymbol{\Phi}\mathbf{V})^T\right) \tag{9}$$

$$\mathbf{V} = (\boldsymbol{\Phi}^T\mathbf{M}_A\boldsymbol{\Phi})^{-1}\boldsymbol{\Phi}^T\mathbf{M}_A \tag{10}$$

The new variables $\bar{\mathbf{K}}_A$ and $\bar{\mathbf{M}}_A$ are defined as $\boldsymbol{\Phi}^T\mathbf{K}_A\boldsymbol{\Phi}$ and $\boldsymbol{\Phi}^T\mathbf{M}_A\boldsymbol{\Phi}$, respectively. Once again, the experimental shapes must be expanded to the full finite element degrees of freedom. In this case study, the SEREP technique is used to perform the expansion.

$$\mathbf{T}_{SEREP} = \boldsymbol{\Phi}_{fem}\boldsymbol{\Phi}^{+}_{a,fem} \tag{11}$$

$$\boldsymbol{\Phi} = \mathbf{T}_{SEREP}\boldsymbol{\Phi}_{\boldsymbol{a}} \tag{12}$$

Where $\boldsymbol{\Phi}_{fem}$ is the first 100 mode shapes of the FEM at the full set of degrees of freedom and $\boldsymbol{\Phi}_{a,fem}$ represents the same matrix partitioned to only the measurement set of degrees of freedom. Note that the SEREP updating also performs

smoothing of the experimental data, so no additional smoothing step was performed here. Using the lesson learned from the previous approach, the FEM rigid body modes were used along with the experimental shapes in the updating procedure.

As in the first approach, the eigenvalue problem was solved with the updated mass and stiffness matrix to verify that the natural frequencies and mode shapes exactly matched the test data. Figure 13 shows a representative frequency response function.

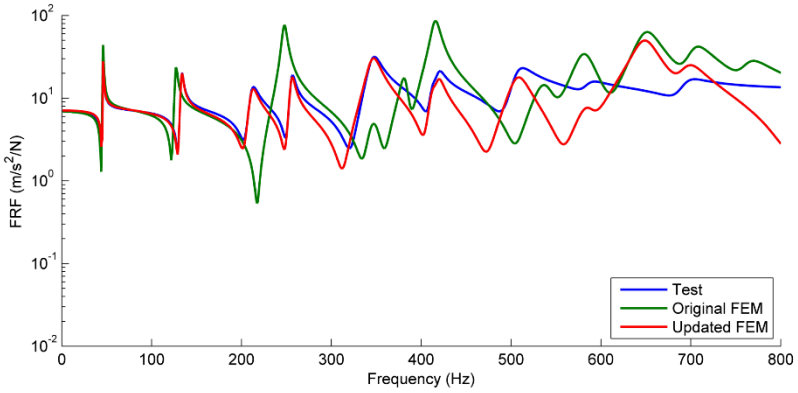


**Figure 13: Representative frequency response function for the updated FEM via the AMI approach.**

Again base of the blade was fixed and the natural frequencies of this new system were found. The first three are shown in Table 3.

**Table 3: Fixed-base FEM predictions using the AMI approach. The truth column contains the average of the natural frequencies found in [6].**

| Mode | Truth | Non-updated FEM | Updated FEM |
|---|---|---|---|
| 1 | 20.1 Hz | 19.3 Hz | 40.0 Hz |
| 2 | 70.2 Hz | 70.7 Hz | 78.2 Hz |
| 3 | 131 Hz | 141 Hz | 169.9 Hz |

The results from using the SEREP expansion and AMI updating technique are worse than the Berman-Nagy approach using Guyan expansion, and again significantly worse than the preliminary FEM.

### 4.3 Variability Improvement of Key Inaccurate Node Groups

The previous approaches utilized the full FEM matrix with updating, and additionally used the entire (smoothed) experimental shape to perform the updating. However, all of these approaches seemed to give poor results when the resulting FEM matrices were assembled to a different structure. The VIKING technique uses a different approach, noting that some degrees of freedom will be measured less accurately than others in any given mode, and instead uses only the best measured degrees of freedom to smooth the variation observed in measured data [10].

For each mode shape the degrees of freedom that are determined to be accurately measured are used in the expansion process. The degrees of freedom are judged by their contribution to the unit value on the diagonal of (13). The degrees of freedom with the largest contribution towards the unit diagonal are kept, up to 99%, resulting in approximately 400-600 of the ~1100 experimental degrees of freedom being kept, referred to in this paper as the $v$ set. Note that the $v$ degrees of freedom vary from mode to mode. Figure 14 shows a representative curve showing degree of freedom contributions with the 99% cutoff marked.

$$\mathbf{I} = \mathbf{\Phi}_a^{+}\mathbf{\Phi}_a \tag{13}$$

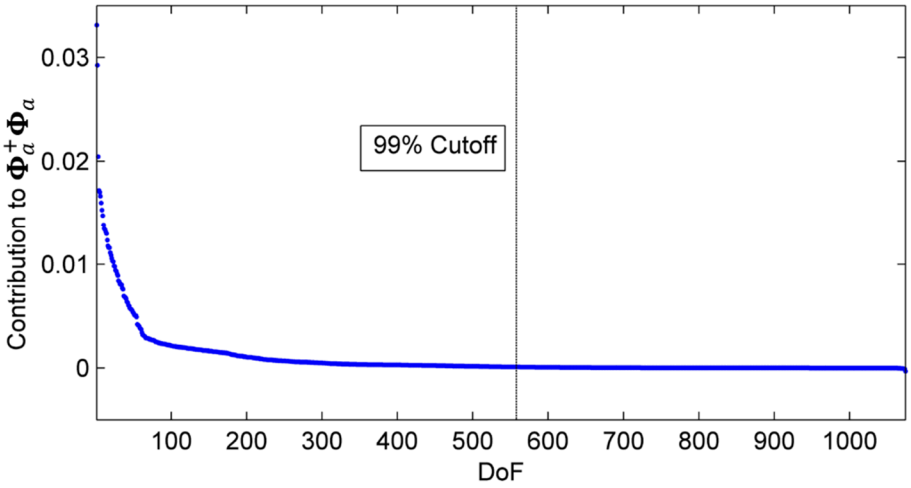


**Figure 14: Degree of freedom contribution to (13).**

One the degrees of freedom have been selected for each mode, the SEREP expansion procedure (11) is used, except instead of performing the expansion using the entire $a$ set of degrees of freedom, only the $v$ subset is used for each mode.

$$\phi = \mathbf{\Phi}_{fem}\mathbf{\Phi}_{v,fem}^{+}\phi_v \tag{14}$$

where $\phi$ represents a single modal vector (because the $v$ set changes with each mode). Equation (14) is performed for each experimental mode using 25 FEM mode shapes as the filter. These then are the finite element mode shapes $\mathbf{\Phi}$ that are used in the AMI procedure (8)-(10). The mass and stiffness matrices were updated and the eigenvalue problem was solved to verify that the natural frequencies exactly matched test data. A representative frequency response function is shown in Figure 15. One other noteworthy aspect is that it appears that the mass line of the FRF has changed. The substructuring exercise was repeated and results are shown in Table 4. It is clear from these results that the VIKING approach significantly improves the substructure model of the turbine blade; however, it is still a bit poorer than if the model had had no updating at all. A brief investigation was performed to see whether or not these results could be improved by tuning the VIKING analysis parameters.

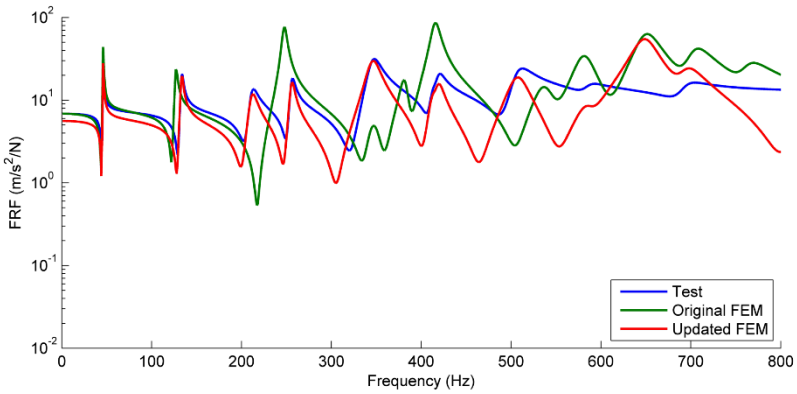


**Figure 15: Representative frequency response function for the updated FEM using the VIKING approach.**

**Table 4: Fixed-base FEM predictions using the VIKING-AMI approach. The truth column contains the average of the natural frequencies found in [6].**

| Mode | Truth | Non-updated FEM | Updated FEM |
|---|---|---|---|
| 1 | 20.1 Hz | 19.3 Hz | 22.3 Hz |
| 2 | 70.2 Hz | 70.7 Hz | 73.7 Hz |
| 3 | 131 Hz | 141 Hz | 149.2 Hz |

## 5 VIKING DISCUSSION

The VIKING and SEREP approaches have some parameters that need to be specified by the analyst performing the model updating, namely the degrees of freedom to keep in the $v$ set (or proportion of the contribution to the unit diagonal that should be kept), and the number of finite element modes to use in the SEREP updating in (14). Additionally, the finite element model matrix could be reduced prior to updating as has been typically done with the VIKING technique [9,10]. A handful of cases were run that varied these parameters.

In one example, the number of modes used in the SEREP expansion was increased to 50, while the number of degrees of freedom kept remained constant at 99% of the contribution to the diagonal of $\boldsymbol{\Phi}_a^+\boldsymbol{\Phi}_a$. The degradation of the results was immediately visible in the MAC comparison between the experiment and the VIKING shapes: the first diagonal term was reduced to 77%. The first predicted fixed base mode using the updated model jumped to 34 Hz, a much poorer prediction.

The number of degrees of freedom were then increased to 99.99% of the contribution to the diagonal of $\boldsymbol{\Phi}_a^+\boldsymbol{\Phi}_a$ to see if this could compensate for the increased number of modes kept in the SEREP filter. The MAC correlation between the experiment and VIKING shapes improved such that the minimum diagonal value was now 97%. The prediction of the first fixed-base mode improved to 23.0 Hz. This is still not quite as good of a prediction as the parameters discussed in Section 4.3, which suggests including too many modes can degrade the results.

Keeping more degrees of freedom than necessary also degraded the results, as these non-accurate degrees of freedom only serve to confuse the updating procedure. If degrees of freedom corresponding to 99.99% of the contributions to the diagonal of $\boldsymbol{\Phi}_a^+\boldsymbol{\Phi}_a$ were kept, but only 25 modes were used in the SEREP expansion, the updated prediction of the first fixed base natural frequency remained 23.0 Hz. If 100% of the contributions to the diagonal of $\boldsymbol{\Phi}_a^+\boldsymbol{\Phi}_a$ (i.e. all of the degrees of freedom) were used, then the case becomes identical to that in Section 4.2, and the results are more severely degraded.

Finally, two sets of reduced order models were run using Guyan reduction to reduce to a smaller set of degrees of freedom in the finite element model, as was done in [10], where good results were obtained in a similar substructuring example. The first reduction simply reduced out the rotational degrees of freedom from the shell elements in the FEM. Using the same parameters as in Section 4.3, the reduced FEM predicted similar fixed base natural frequencies as that approach. A more severe reduction was performed, reducing the FEM down to only the experimental measurement nodes as well as 17 nodes scattered around the clamped section of the blade to provide degrees of freedom to constrain for the fixed base approach. This approach actually obtained the best results with predicted fixed base natural frequencies of 21.6, 69.1, and 133.5 Hz. This was the only approach that improved upon the preliminary FEM in terms of predicting fixed base natural frequencies.

## 6 SUMMARY

Three case studies were performed using model updating techniques on an Ampair 600 Wind Turbine Blade with the goal of updating the finite element model to more closely match test data. The preliminary model matched test data reasonably well after tuning the elastic moduli of the materials, though it did not exactly match test data. Test data could be exactly matched after all three updating procedures; however very different results were obtained when the finite element model was fixed at the base and the modes of that configuration were solved for. The Berman-Nagy updating approach with Guyan expansion and AMI approach with SEREP expansion both resulted in models that predicted wildly inaccurate fixed base modes. Only when the VIKING technique was utilized were more reasonable results obtained. However, as judged by the metric in this paper, the preliminary model still performed the best in predicting the fixed base natural frequencies.

## 7 REFERENCES


[1] Baruch, M., "Optimal correction of mass and stiffness matrices using measured modes", AIAA Journal, Vol. 20, No. 11 (1982), pp. 1623-1626.

[2] Berman, A. and Nagy, E. J., "Improvement of a Large Analytical Model Using Test Data", AIAA Journal, Vol. 21, No. 8 (1983), pp. 1168-1173.

[3] O'Callahan, J. and Leung, R., "Optimization of mass and stiffness matrices using a generalized inverse technique on the measured modes", *Proceedings of the 3rd International Modal Analysis Conference*, pp.75-79, Orlando, Fl., 1985.

[4] Castellini, P., Martarelli, M., and Tomasini, E.P., "Laser Doppler Vibrometry: Development of advanced solutions answering to technology's needs", *Mechanical Systems and Signal Processing*, Volume 20, Issue 6, p. 1265-1285, 2006.

[5] Mayes, R. L., "An Introduction to the SEM Substructures Focus Group Test Bed – The Ampair 600 Wind Turbine",

*Proceedings of the 30th International Modal Analysis Conference.* pp. 61–71, 2012.

[6] Harvie, J. and Avitabile, P., "Comparison of Some Wind Turbine Blade Tests in Various Configurations". *Proceedings of the 30th International Modal Analysis Conference,* pp. 71–72, 2012.

[7] Nurbhai, M. S. and Macknelly, D. J., "Modal Assessment of Wind Turbine Blade in Preparation of Experimental Substructuring", *Proceedings of the 30th International Modal Analysis Conference,* pp. 73–79, 2012.

[8] Hensley, Daniel P., and Mayes, Randall L., "Extending SMAC to Multiple References", *Proceedings of the 24th International Modal Analysis Conference,* pp.220-230, February 2006.

[9] Thibault, L., Butland, A., and Avitabile, P., "Variability Improvement of Key Inaccurate Node Groups – VIKING", *Proceedings of the 30th International Modal Analysis Conference,* 2012.

[10] Butland, A. and Avitabile, P., "Component Mode Synthesis using Reduced Order, Test Verified Components", *Proceedings of the 27th International Modal Analysis Conference,* 2009.

[11] Allen, M. S., Kammer, D. C., and Mayes, R. L., "Uncertainty in Experimental/Analytical Substructuring Predictions: A Review with Illustrative Examples", *Proceedings of the International Conference on Noise and Vibration Engineering,* Leuven, Belgium, 2010.